Crystal structure of meglumine diatrizoate, $(C_7H_{18}NO_5)(C_{11}H_8I_3N_2O_4)$

Tawnee M. Ens,[1] James A. Kaduk,[1,2,a] Anya Vieira Dosen,[3] and Thomas N. Blanton[3]
[1]*North Central College, 131 S. Loomis St., Naperville, IL 60540, USA*
[2]*Illinois Institute of Technology, 3101 S. Dearborn St., Chicago, IL 60616, USA*
[3]*ICDD, 12 Campus Blvd., Newtown Square, PA 19073-3273, USA*

(Received 14 February 2023; accepted 30 April 2023)

The crystal structure of meglumine diatrizoate has been solved and refined using synchrotron X-ray powder diffraction data and optimized using density functional theory techniques. Meglumine diatrizoate crystallizes in space group $P2_1$ (#4) with $a = 10.74697(4)$, $b = 6.49364(2)$, $c = 18.52774(7)$ Å, $\beta = 90.2263(3)$, $V = 1292.985(5)$ Å^3, and $Z = 2$. Two different crystal structures, which yielded essentially identical refinement residuals and positions of the non-H atoms, were obtained. The differences were in the H atom positions and the hydrogen bonding. One structure was 123.0 kJ/mol/cell lower in energy than the other and was adopted for the final description. The crystal structure consists of alternating double layers of cations and anions along the *c*-axis. The hydrogen bonds link the cations and anions into a three-dimensional framework. Each of the hydrogen atoms on the ammonium nitrogen of the cation acts as a donor in a strong N–H···O hydrogen bond. One of these is to a hydroxyl group of another cation, and the other is to the carboxylate group of the anion. Each of the amide nitrogen atoms of the anion forms a strong N–H···O intermolecular hydrogen bond, one to a carbonyl and the other to a carboxylate group. The powder pattern has been submitted to ICDD for inclusion in the Powder Diffraction File™ (PDF®).

[doi:10.1017/S0885715623000180]

Key words: meglumine diatrizoate, renografin, crystal structure, Rietveld refinement, density functional theory

I. INTRODUCTION

Meglumine diatrizoate (combined with diatrizoate sodium and sold under the brand name Renografin-60 and Gastrografin, among others) is a common colorless liquid contrast agent used in radiography, commonly of the urinary tract and parts of the digestive system, and is administered orally or intravascularly (Geng et al., 2018). The systematic name (CAS Registry Number 131-49-7) is (2R,3R,4R,5S)-6-(methylammonium)hexane-1,2,3,4,5-pentol 3,5-diacetamido-2,4,6-triiodobenzoate. For children and adults, 660 mg/ml of meglumine diatrizoate is used with 100 mg/ml diatrizoate sodium as an injection and is named MD-76R by the FDA (Dizendorf et al., 2002; FDA.gov, 2017). There are a number of possible side effects of MD-76R, including a decrease in urine production or blood in urine, burning sensation and pain during urination, dizziness, increased heart rate, and others (Mayo Clinic, 2022). The effect of nephrotoxicity due to meglumine diatrizoate and other contrast agents has also been presented, particularly in angioplasty and angiography (Berns, 1989). A two-dimensional molecular diagram is shown in Figure 1.

A connectivity search for the meglumine cation in the Cambridge Structural Database (Groom et al., 2016) yielded two hits: meglumine (2R,4E)-7-chloro-4-(2-oxo-1-phenyl-3-pyrrolidinylidene)-1,2,3,4-tetrahydro-2-quinolinecarboxylic acid (Di Fabio et al., 2002; HUTMAK) and (2S,3R,4R,5R)-2,3,4,5,6-pentahydroxy-N-methyl-1-hexanaminium 2-(2-methyl-3-(trifluoromethyl)anilino)nicotinate (Cao et al., 2003; ILIQID). Similar searches for diatrizoic acid and its derivatives yielded crystal structures of the free acid (Fucke et al., 2015; PUFJUX), several hydrates and solvates (Fucke et al., 2012; ECEZOD, ECEZUJ, ECIBAV; Fucke et al., 2015; PUFGUU, PUFGUU01, PUFJIL, PUFJUX, PUFKEI, PUFKOS, PUFLAF, PUFLIN), several hydrated/solvated sodium salts (Najib et al., 2017; CERRID, CERROJ, CERRUP, CERSAW; Fucke et al., 2015; PUFHOP, PUFHOP01), and several lanthanide salts.

Meglumine diatrizoate is claimed as a component of oral contrast agents in US Patent 7,384,624 B2 (Raines, 2008) and is described as useful in radiosurgery of tumors in US Patent Application 2004/0006254 A1 (Weil and Morris, 2004). We are unaware of any published X-ray powder diffraction data on meglumine diatrizoate.

This work was carried out as part of a project (Kaduk et al., 2014) to determine the crystal structures of large-volume commercial pharmaceuticals and include high-quality powder diffraction data for them in the powder diffraction file (PDF) (Gates-Rector and Blanton, 2019).

[a]Author to whom correspondence should be addressed. Electronic mail: kaduk@polycrystallography.com

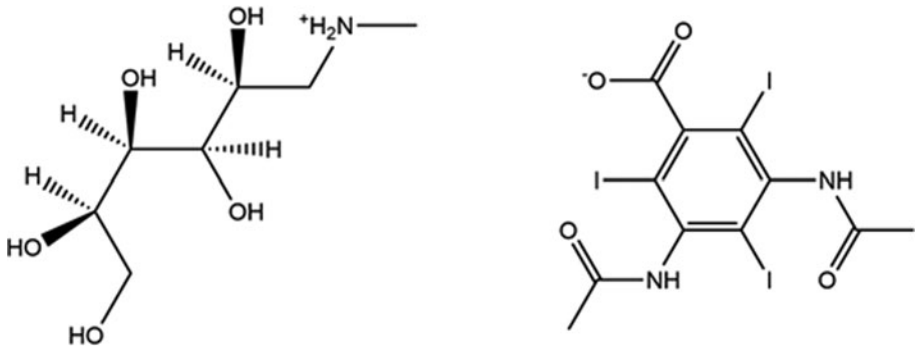

Figure 1. The 2D molecular structure of meglumine diatrizoate.

II. EXPERIMENTAL

Meglumine diatrizoate was a commercial reagent, purchased from Sigma (Batch #SLCJ2134), and was used as-received. The white powder was packed into a 1.5 mm diameter Kapton capillary and rotated during the measurement at ~50 Hz. The powder pattern was measured at 295 K at beam line 11-BM (Antao et al., 2008; Lee et al., 2008; Wang et al., 2008) of the Advanced Photon Source at Argonne National Laboratory using a wavelength of 0.458963(2) Å from 0.5 to 50° 2θ with a step size of 0.001° and a counting time of 0.1 s/step. The high-resolution powder diffraction data were collected using 12 silicon crystal analyzers that allow for high angular resolution, high precision, and accurate peak positions. A mixture of silicon (NIST SRM 640c) and alumina (NIST SRM 676a) standards (ratio Al_2O_3:Si = 2:1 by weight) was used to calibrate the instrument and refine the monochromatic wavelength used in the experiment. The beamline staff noted that the meglumine diatrizoate specimen changed slightly during the measurement.

The synchrotron diffraction pattern was indexed using N-TREOR (Altomare et al., 2013) on a high-quality primitive monoclinic unit cell with $a = 10.74782$, $b = 6.49318$, $c = 18.53081$ Å, $\beta = 90.206°$, $V = 1293.2$ Å^3, and $Z = 2$. A reduced cell search of the Cambridge Structural Database (Groom et al., 2016) with the chemistry C, H, I, N, and O only, yielded no hits.

The meglumine cation was extracted from the previously mentioned HUTMAK crystal structure using *Materials Studio* (Dassault Systèmes, 2021), and saved as a *.mol2 file. This file was converted to a Fenske–Hall *Z*-matrix using OpenBabel (O'Boyle et al., 2011). The diatrizoate anion was built using *Spartan '18* (Wavefunction, 2020), saved as a *.mol2 file, and converted using the same tools as for the cation.

The structure was solved using Monte Carlo simulated annealing techniques as implemented in EXPO2014 (Altomare et al., 2013) and FOX (Favre-Nicolin and Černý, 2002). Two different structures (structures 1 and 2) were obtained. Both had similar arrangements of heavy (non-H) atoms, but different apparent H-bonding patterns. We refined and optimized both structures. Although both structures refined to similar residuals ($R_{wp} = 0.04566$ and 0.04556 and goodness of fit (GOF) = 1.58 and 1.57 for structures 1 and 2, respectively), the (VASP) energy of structure 2 was 123.0 kJ/mol/cell lower in energy than that of structure 1, so is the one primarily discussed here.

Rietveld refinement was carried out using general Structure Analysis System (GSAS)-II (Toby and Von Dreele, 2013). Only the 1.0–30.0° portion of the pattern was included in the refinement ($d_{min} = 0.887$ Å). All non-H bond distances and angles were subjected to restraints, based on a Mercury/Mogul Geometry check (Bruno et al., 2004; Sykes et al., 2011). The Mogul average and standard deviation for each quantity were used as the restraint parameters. The restraints contributed 1.7% to the final χ^2. The hydrogen atoms were included in calculated positions, which were recalculated during the refinement using Materials Studio (Dassault Systèmes, 2021). The I atoms were refined anisotropically. The U_{iso} of the heavy atoms was grouped by chemical similarity. The U_{iso} for the H atoms was fixed at 1.3× the U_{iso} of the heavy atoms to which they are attached. No preferred orientation model was included in the refinement. The peak profiles were described using the generalized microstrain model (Stephens, 1999). The background was modeled using a six-term shifted Chebyshev polynomial, and a peak at 6.18° 2θ to model the scattering from the Kapton capillary and an amorphous component.

The final refinement of 141 variables using 29,047 observations and 76 restraints yielded the residuals $R_{wp} = 0.0456$ and GOF = 1.57. The largest peak (1.65 Å from O48) and hole (1.47 Å from I38) in the difference Fourier map were 0.37(9) and –0.41(9) eÅ^{-3}, respectively. The largest errors in the difference plot (Figure 2) are in the shapes of some of the low-angle peaks, perhaps reflecting the specimen changes noted by the beamline staff.

Both structures of meglumine diatrizoate were optimized (fixed experimental unit cell) with density functional techniques using VASP (Kresse and Furthmüller, 1996) through the MedeA graphical interface (Materials Design, 2016). The calculations were carried out on 16 2.4 GHz processors (each with 4 Gb RAM) of a 64-processor HP Proliant DL580 Generation 7 Linux cluster at North Central College. The calculation used the generalized gradient approximation (GGA)-Perdew-Burke-Ernzerhof (PBE) functional, a plane wave cutoff energy of 400.0 eV, and a *k*-point spacing of 0.5 Å^{-1} leading to a 2 × 2 × 1 mesh, and took ~19 (structure 1) and 10 (structure 2) hours. Single-point density functional calculations (fixed experimental cell) and population analysis were carried out using CRYSTAL17 (Dovesi et al., 2018). The basis sets for the H, C, N, and O atoms in the calculation were those of Gatti et al. (1994), and for I was that of Laun and Bredow (2022). The calculations were run on a 3.5 GHz PC using 8 *k*-points and the B3LYP functional and took ~2.8 h.

https://doi.org/10.1017/S0885715623000180 Published online by Cambridge University Press

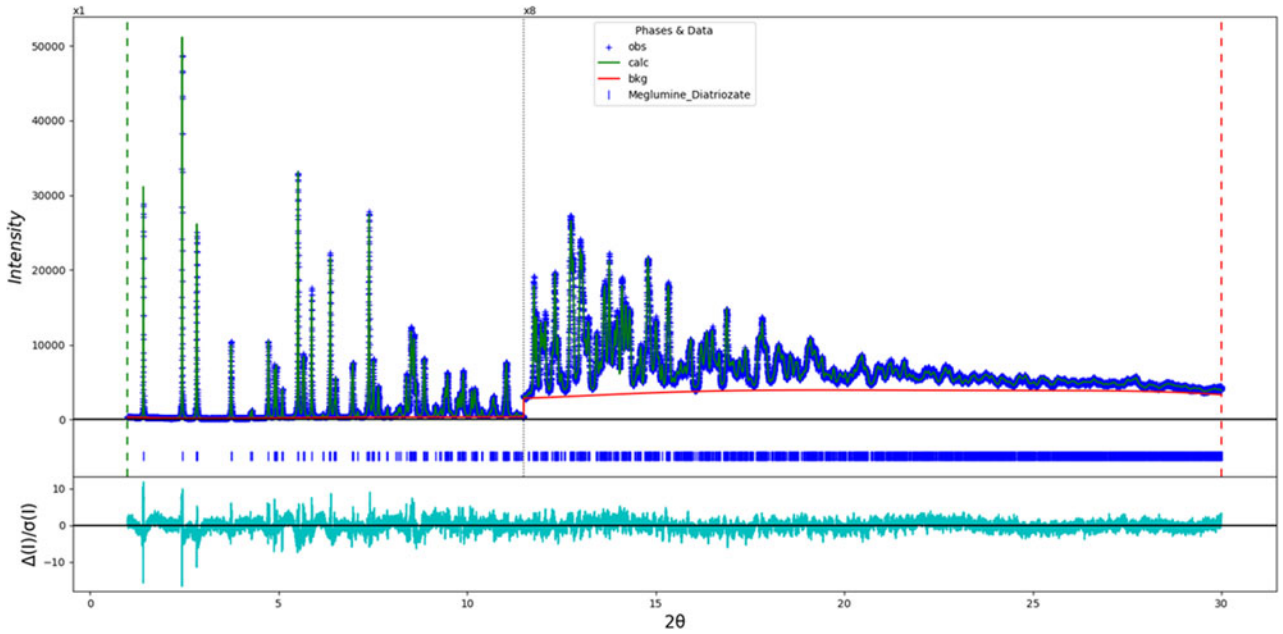

Figure 2. The Rietveld plot for the refinement of meglumine diatrizoate. The blue crosses represent the observed data points, and the green line is the calculated pattern. The cyan curve is the normalized error plot, and the red line is the background curve. The vertical scale has been multiplied by a factor of 8× for $2\theta > 12.0°$.

III. RESULTS AND DISCUSSION

Two different crystal structures of meglumine diatrizoate, which yielded essentially identical refinement residuals and positions of the non-H atoms, were obtained. The orientations of four of the five hydroxyl groups (O1, O2, O3, and O4) in the meglumine cation differ between the two structures (Figure 3). Some of the atoms have different names in the two structures. There is an additional complication in describing the structures. The chemical connectivity of the anion exhibits two-fold rotational symmetry, but the atom names are arbitrary. Superposition of the anions of the two structures (Figure 4) reveals that the structure solutions oriented the anions differently, so that chemically-equivalent atoms bear different atom numbers in the two structures. The DFT calculations indicated that structure 2 was significantly lower in energy, so is preferred and the one on which this discussion concentrates.

The root-mean-square Cartesian displacement between the Rietveld-refined and DFT-optimized cations is 0.084 Å

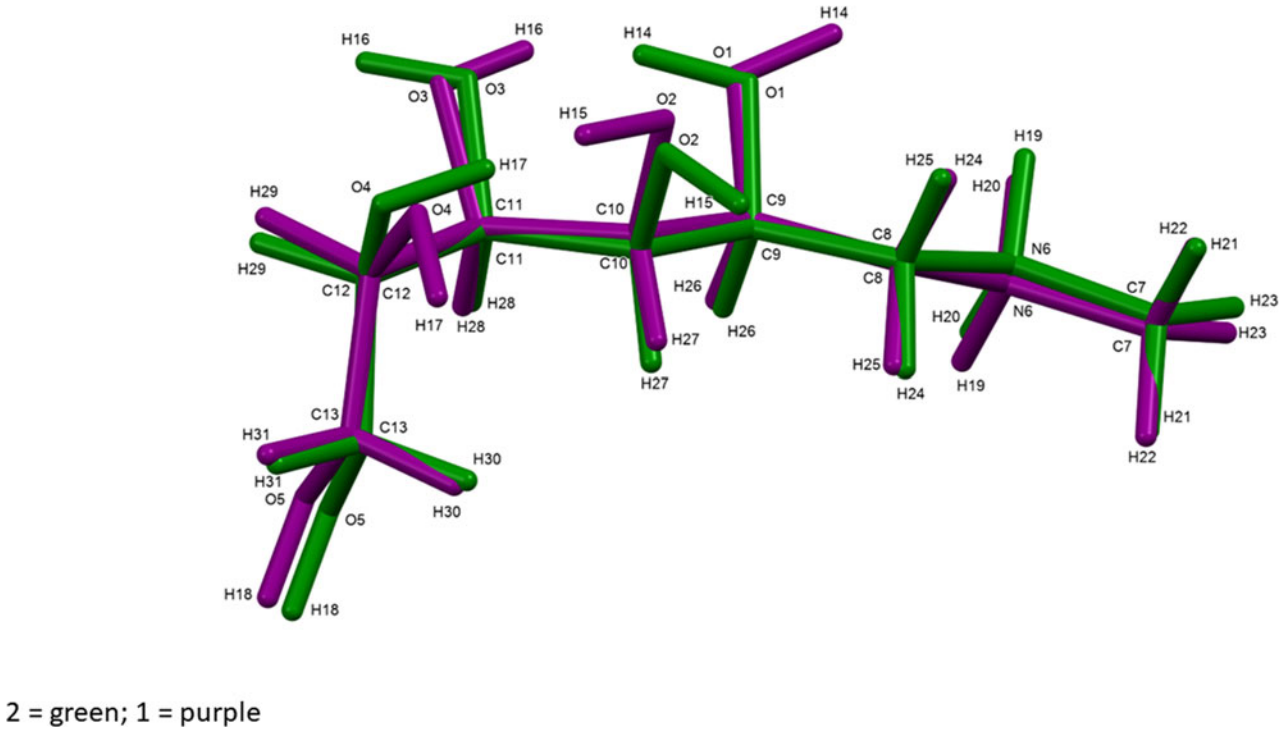

Figure 3. Comparison of the structure of the cation in the correct (low-energy) structure (green) and the incorrect (high-energy) structure (purple). Image generated using Mercury (Macrae et al., 2020).

https://doi.org/10.1017/S0885715623000180 Published online by Cambridge University Press

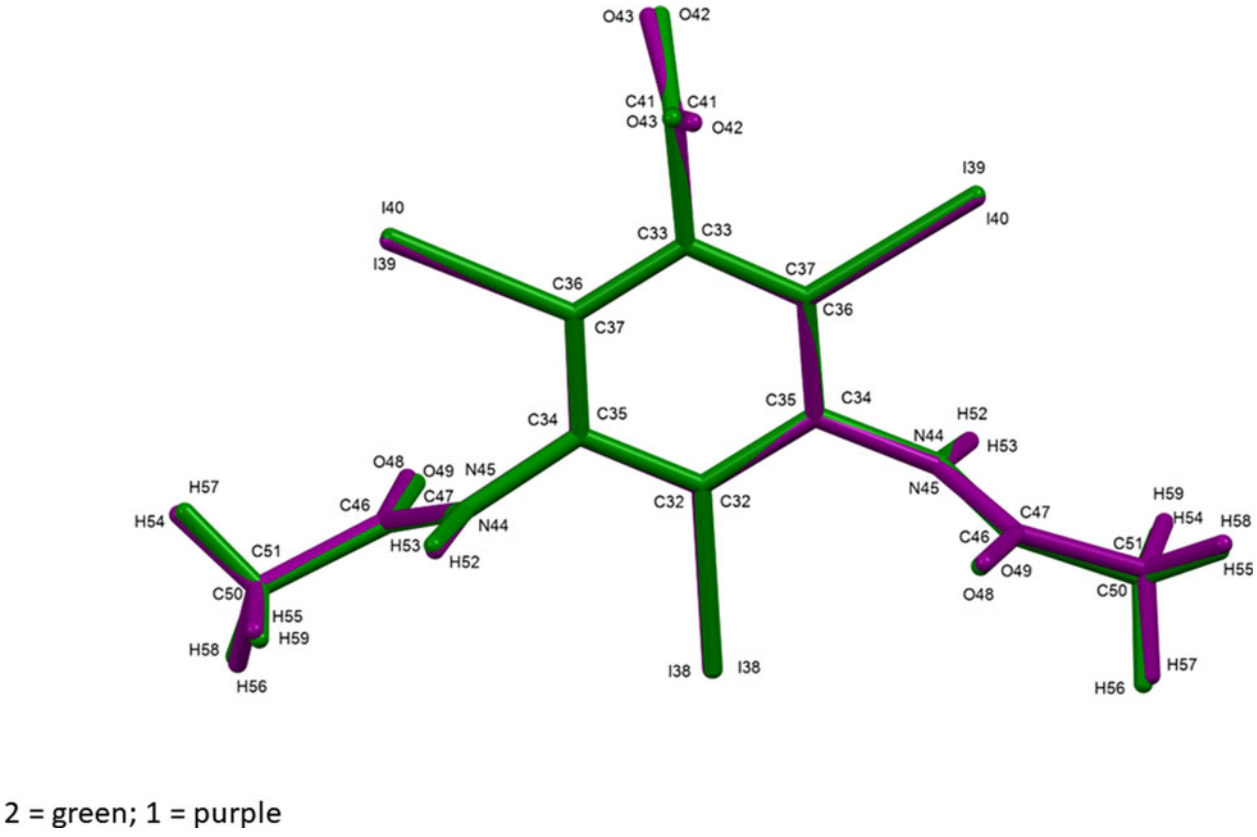

2 = green; 1 = purple

Figure 4. Comparison of the structure of the anion in the correct (low-energy) structure (green) and the incorrect (high-energy) structure (purple). Image generated using Mercury (Macrae et al., 2020).

(Figure 5). The maximum deviation is 0.114 Å, at the methyl group C7. The similar quantities for the anion are 0.053 Å (Figure 6) and 0.100 Å, at C47. The excellent agreement is well within the normal range for correct structures (van de Streek and Neumann, 2014) and provides strong evidence that the refined structure is correct. The asymmetric unit (with atom numbering) is illustrated in Figure 7.

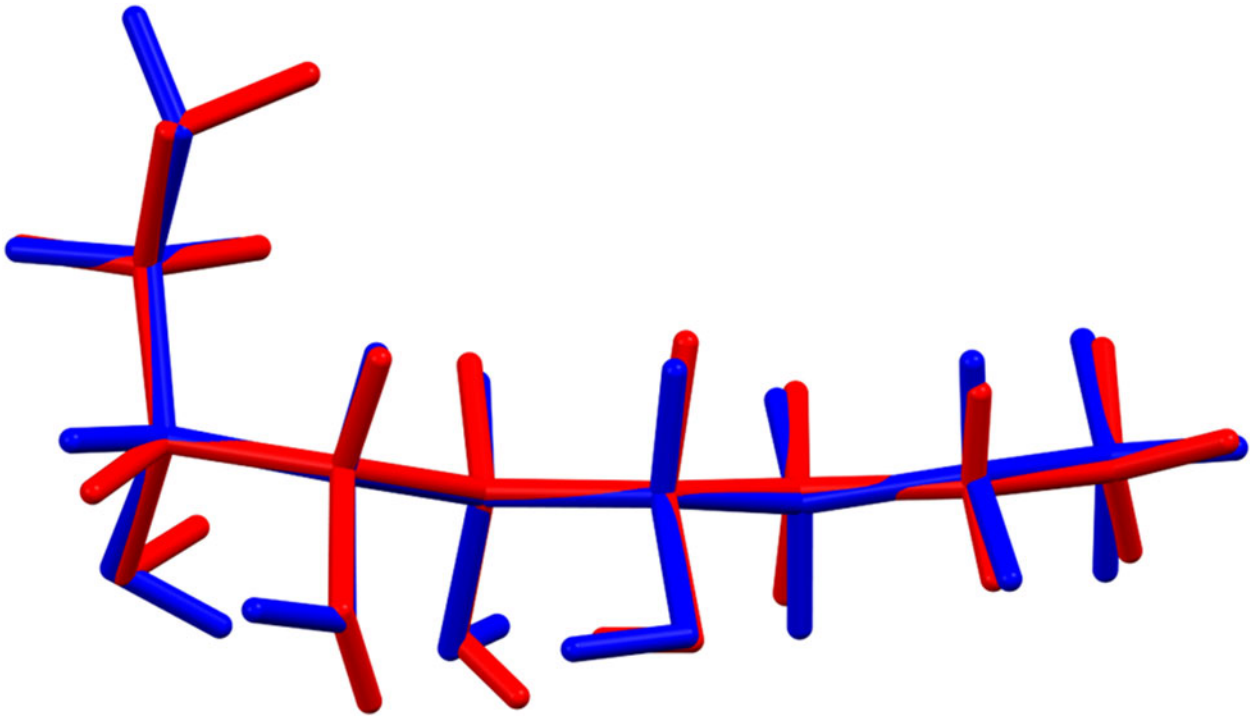

Figure 5. Comparison of the Rietveld-refined (red) and VASP-optimized (blue) structures of the meglumine cation. The rms Cartesian displacement is 0.084 Å. Image generated using Mercury (Macrae et al., 2020).

https://doi.org/10.1017/S0885715623000180 Published online by Cambridge University Press

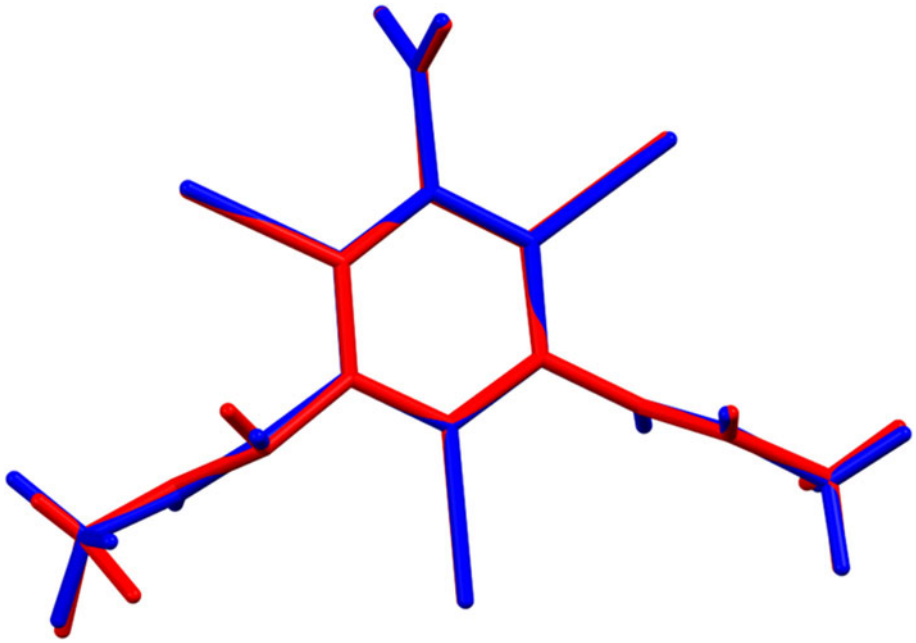

Figure 6. Comparison of the Rietveld-refined (red) and VASP-optimized (blue) structures of the diatrizoate anion. The rms Cartesian displacement is 0.053 Å. Image generated using Mercury (Macrae et al., 2020).

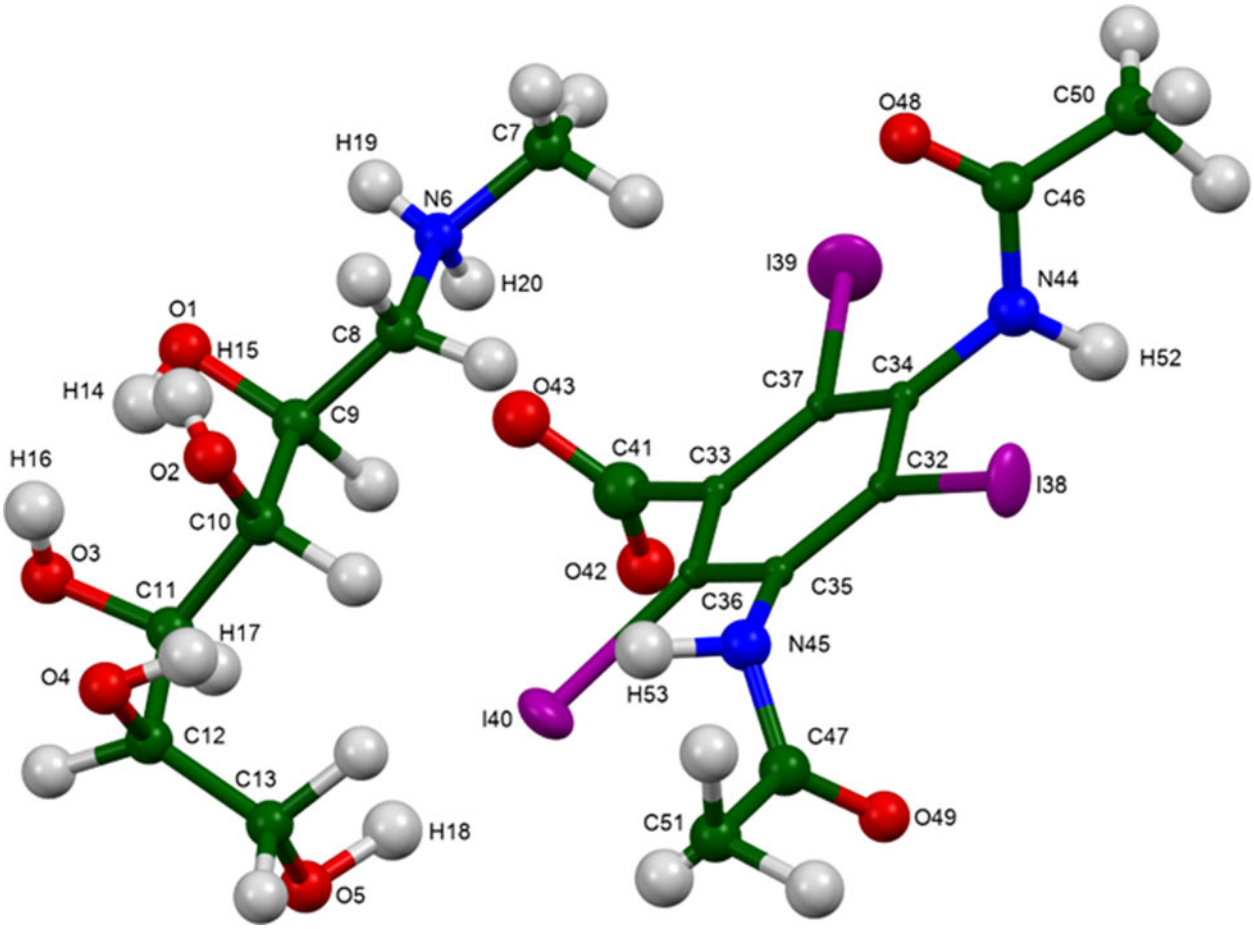

Figure 7. The asymmetric unit of meglumine diatrizoate, with the atom numbering. The atoms are represented by 50% probability spheroids/ellipsoids. Image generated using Mercury (Macrae et al., 2020).

The best view of the crystal structure is down the short *b*-axis (Figure 8). The crystal structure consists of alternating double layers of cations and anions along the *c*-axis. The hydrogen bonds (discussed below) link the cations and anions into a three-dimensional framework. The mean planes of the phenyl rings in the two anions in the unit cell are 3,3,10 and

https://doi.org/10.1017/S0885715623000180 Published online by Cambridge University Press

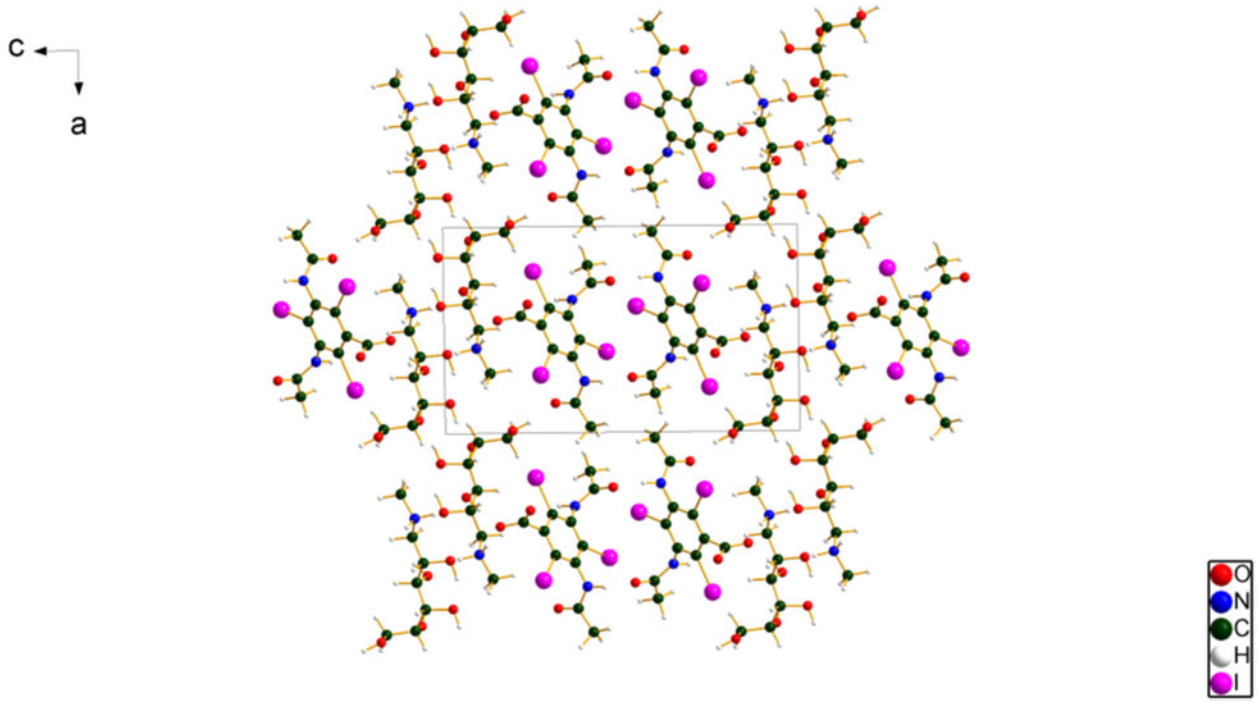

Figure 8. The crystal structure of meglumine diatrizoate, viewed down the *b*-axis. Image generated using Diamond (Crystal Impact, 2022).

3,-3,10. The *Mercury* Aromatics Analyser indicates only two weak interactions with distances of 6.49 and 7.14 Å between the phenyl rings of the anions.

All of the bond distances, bond angles, and torsion angles fall within the normal ranges indicated by a Mercury Mogul Geometry check (Macrae et al., 2020). Quantum chemical geometry optimization of the isolated cation and anion (DFT/B3LYP/6-31G*/water) using Spartan '20 (Wavefunction, 2022) indicated that the observed conformation of the cation is close to a local minimum. The global minimum-energy conformation of the cation differs significantly (Figure 9), and is 41.7 kJ/mol lower in energy. The observed conformation of the anion is very close to a local minimum. The global minimum-energy conformation of the anion is 20.7 kJ/mol lower in energy, and has a very different conformation (Figure 10). The differences are mainly in the conformations of the amide side chains. The differences indicate that intermolecular interactions are important in determining the solid-state conformation.

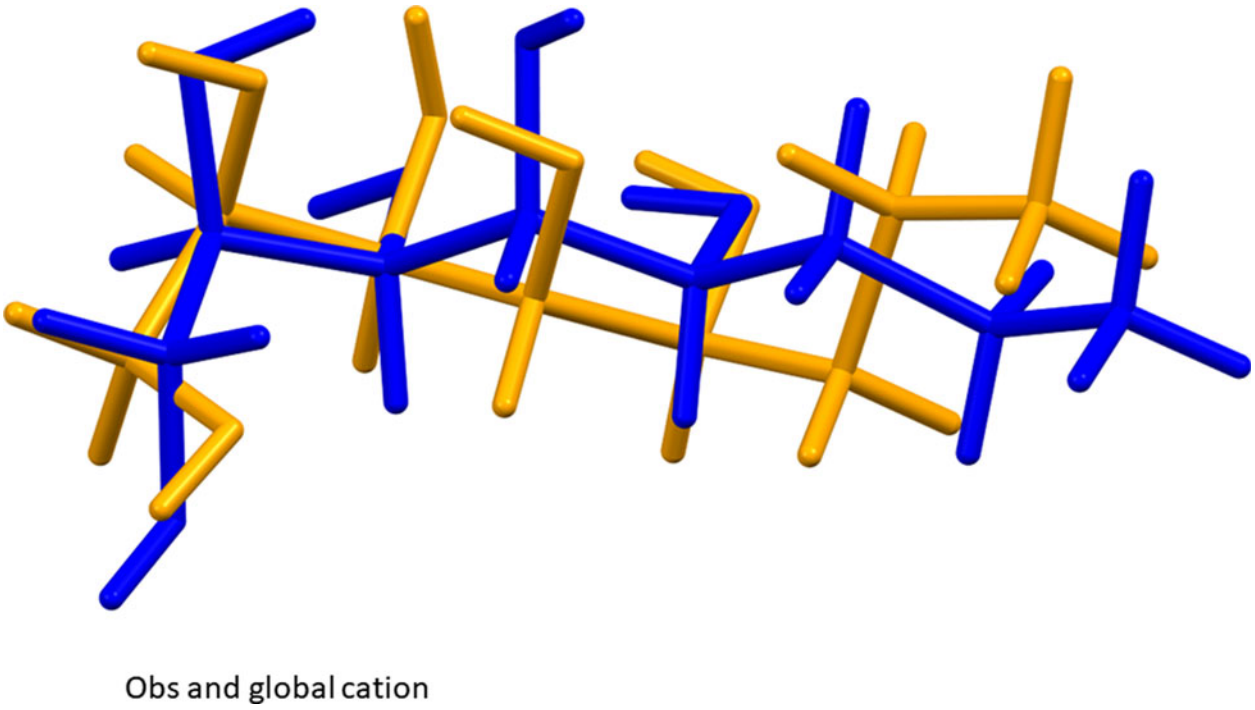

Figure 9. Comparison of the observed structure of the meglumine cation (blue) to the global minimum-energy conformation (orange). Image generated using Mercury (Macrae et al., 2020).

https://doi.org/10.1017/S0885715623000180 Published online by Cambridge University Press

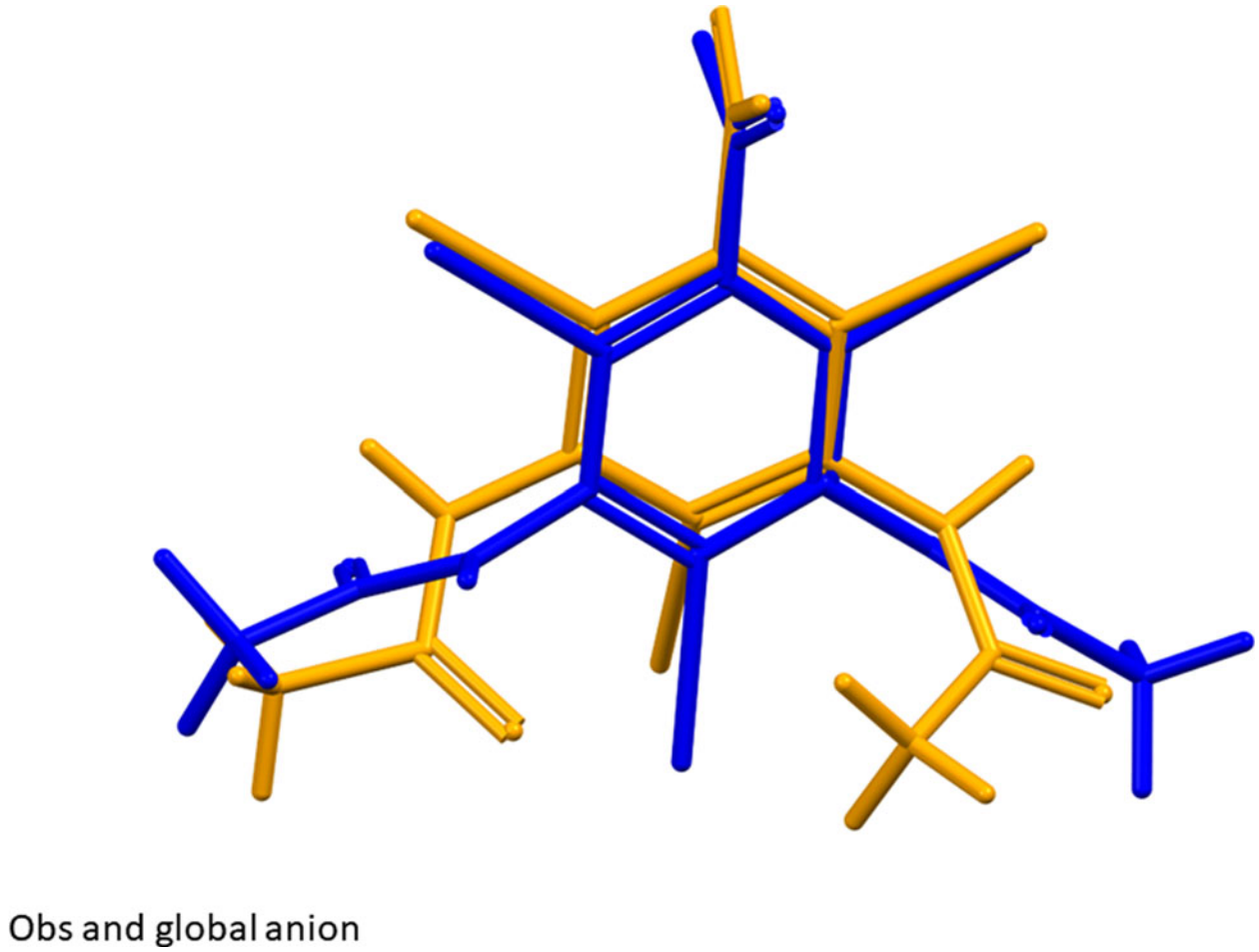

Figure 10. Comparison of the observed structure of the diatrizoate anion (blue) to the global minimum-energy conformation (orange). Image generated using Mercury (Macrae et al., 2020).

Analysis of the contributions to the total crystal energy of the structure using the Forcite module of Materials Studio (Dassault Systèmes, 2021) suggests that torsion distortion terms dominate the intramolecular deformation energy. The intermolecular energy is dominated by electrostatic attractions, which in this force field analysis also include hydrogen bonds. The hydrogen bonds are better analyzed using the results of the DFT calculation.

Hydrogen bonds are prominent in the crystal structure (Table I). Each of the hydrogen atoms on the ammonium

TABLE I. Hydrogen bonds (CRYSTAL17) in the two structure solutions of meglumine diatrizoate.

H-Bond	D–H, Å	H···A, Å	D···A, Å	D–H···A,◦	Overlap, *e*	*E*, kcal/mol
N6–H20/19···O2N6–H19···O2	1.0501.048	1.7821.909	2.7772.921	156.7161.5	0.0680.065	6.05.9
N6–H19/20···O42/43N6–H20···O43	1.0751.057	1.5991.738	2.6672.784	171.4169.2	0.1000.078	7.36.4
N44/45–H52/53···O43/42N45–H53···O42	1.0541.046	1.6501.713	2.6842.734	166.0164.1	0.0850.078	6.76.4
N45/44–H53/52···O48/49N44–H52···O49	1.0411.041	1.8261.821	2.8492.855	166.5171.3	0.0730.070	6.26.1
O1–H14···O2O1–H14···O3	0.9940.992	1.7621.805[a]	2.7462.689	169.5146.7	0.0510.058	12.313.2
O2–H15···O4O2–H15···O43	0.9981.018	1.731[a]1.643	2.6192.660	146.1176.6	0.0690.071	14.414.6
O3–H16···O1O3–H16···O4	0.9821.002	1.979[a]1.687	2.8152.678	141.6169.2	0.0350.063	10.213.7
O4–H17···I39/40O4–H17···O2	0.9790.993	3.0811.805[a]	4.0102.721	158.9151.7	0.0150.063	13.7
O5–H18···O49/48O5–H18···O48	0.9940.995	1.7941.736	2.7732.712	167.3166.2	0.0590.062	13.313.6
C7–H22/21···O49/48	1.096	2.684	3.539	134.4	0.011	
C7–H23···O3C7–H23···O3	1.0941.094	2.6772.465	3.3803.370	121.4139.3	0.0090.017	
C8–H24/25···O1C8–H25···O1	1.0981.100	2.2812.280	3.3023.380	153.8178.1	0.0310.031	
C8–H25/24···O43/42C8–H24···O42	1.0991.100	2.6592.553	3.6003.456	143.2138.6	0.0130.014	
C9–H26···O42/43C9–H26···O43	1.1071.108	2.6852.523	3.4993.374	129.8132.7	0.0100.011	
C10–H27···O43/42C10–H27···O42	1.1041.102	2.1902.265	3.2413.197	158.1141.0	0.0270.020	
C11–H28···O5C11–H28···O5	1.1061.106	2.420[a]2.463[a]	2.9472.939	107.4104.3	0.0090.010	
C13–H31···I40/39C13–H31···I39	1.1071.105	3.1222.956	4.0713.931	144.1147.3	0.0100.013	

The top lines are structure 1 (incorrect/higher energy) and the bottom lines are structure 2 (correct/lower energy). XXX structure 1 to structure 2 equivalent names.
[a]Intramolecular.

https://doi.org/10.1017/S0885715623000180 Published online by Cambridge University Press

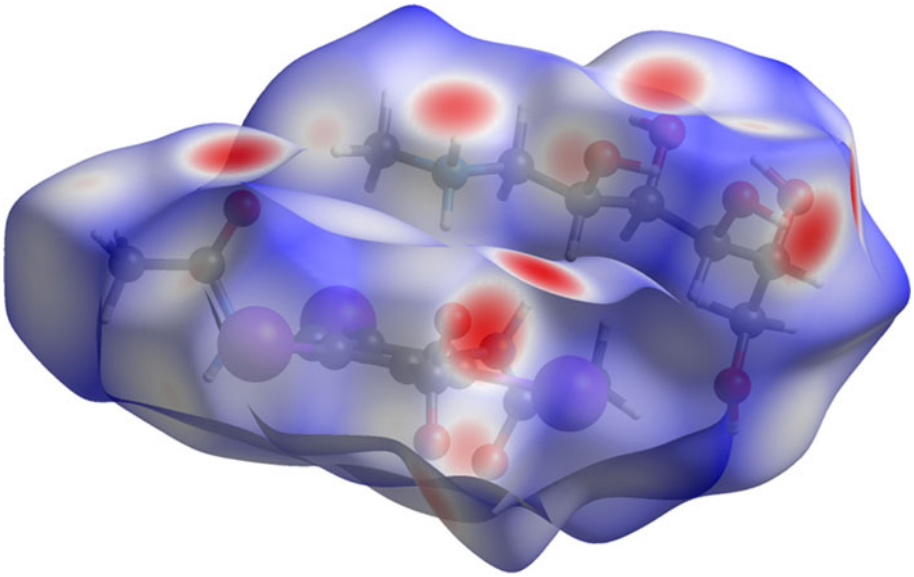

Figure 11. The Hirshfeld surface of meglumine diatrizoate. Intermolecular contacts longer than the sums of the van der Waals radii are colored blue, and contacts shorter than the sums of the radii are colored red. Contacts equal to the sums of radii are white. Image generated using CrystalExplorer (Spackman et al., 2021).

TABLE II. C–I···O halogen bonds (CRYSTAL17) in meglumine diatrizoate

Bond	C–I, Å	I···O, Å	C–I···O,°	Overlap, *e*
C32–I38···O49	2.101	3.122	163.3	0.016
C37–I39···O48	2.102	3.441	146.3	0.006
C36–I40···O5	2.114	2.978	160.6	0.022

nitrogen N6 of the cation acts as a donor in a strong N–H···O hydrogen bond. One of these is to a hydroxyl group O2 of another cation, and the other is to the carboxylate O43 of the anion. The energies of the N–H···O hydrogen bonds were calculated using the correlation of Wheatley and Kaduk (2019). Each of the amides N44 and N45 of the anion forms a strong N–H···O intermolecular hydrogen bond, one to a carbonyl O49 and the other to a carboxylate O42. Thus, each O of the carboxylate acts as an acceptor in an N–H···O hydrogen bond. There is a variety of O–H···O hydrogen bonds between the hydroxyl groups of the cation. Some are intramolecular to other hydroxyl groups, and others are intermolecular, both to hydroxyl groups and to carboxyl and carbonyl groups. The energies of the O–H···O hydrogen bonds were calculated using the correlation of Rammohan and Kaduk (2018). Several C–H···O hydrogen bonds also contribute to the lattice energy. C–I···O halogen bonds (Table II; Corradi et al., 2000; Wilcken et al., 2013) also apparently contribute to the crystal energy.

The volume enclosed by the Hirshfeld surface of the meglumine diatrizoate asymmetric unit (Figure 11, Hirshfeld, 1977; Spackman et al., 2021) is 637.73 Å^3, 98.64% of 1/2 the unit cell volume. The packing density is thus fairly typical. The only significant close contacts (red in Figure 11) involve the hydrogen bonds. The volume/non-hydrogen atom is larger than normal, at 19.6 Å^3, reflecting the presence of the large I atoms.

The Bravais–Friedel–Donnay–Harker (Bravais, 1866; Friedel, 1907; Donnay and Harker, 1937) morphology suggests that we might expect platy morphology for meglumine diatrizoate, with {001} as the principal faces. No preferred orientation model was necessary, indicating that preferred orientation was not present in this rotated capillary specimen.

IV. DEPOSITED DATA

The powder pattern of meglumine diatrizoate from this synchrotron data set has been submitted to ICDD for inclusion in the PDF. The Crystallographic Information Framework (CIF) files containing the results of the Rietveld refinement (including the raw data) and the DFT geometry optimization were deposited with the ICDD. The data can be requested at pdj@icdd.com.

ACKNOWLEDGEMENTS

Use of the Advanced Photon Source at Argonne National Laboratory was supported by the U. S. Department of Energy, Office of Science, Office of Basic Energy Sciences, under Contract No. DE-AC02-06CH11357. This work was partially supported by the International Centre for Diffraction Data. We thank Lynn Ribaud and Saul Lapidus for their assistance in the data collection.

CONFLICTS OF INTEREST

The authors have no conflicts of interest to declare.

REFERENCES

Altomare, A., C. Cuocci, C. Giacovazzo, A. Moliterni, R. Rizzi, N. Corriero, and A. Falcicchio. 2013. "EXPO2013: A Kit of Tools for Phasing Crystal Structures from Powder Data." *Journal of Applied Crystallography* 46, 1231–35.

Antao, S. M., I. Hassan, J. Wang, P. L. Lee, and B. H. Toby. 2008. "State-of-the-Art High-Resolution Powder X-Ray Diffraction (HRPXRD) Illustrated with Rietveld Refinement of Quartz, Sodalite, Tremolite, and Meionite." *Canadian Mineralogist* 46, 1501–09.

Berns, A. S. 1989. "Nephrotoxicity of Contrast Media." *Kidney International* 36, 730–40. doi:10.1038/ki.1989.254.

Bravais, A. 1866. *Etudes Cristallographiques*. Paris: Gauthier Villars.

Bruno, I. J., J. C. Cole, M. Kessler, J. Luo, W. D. Sam Motherwell, L. H. Purkis, B. R. Smith, R. Taylor, R. I. Cooper, S. E. Harris, and A. Guy Orpen. 2004. "Retrieval of Crystallographically-Derived Molecular Geometry Information." *Journal of Chemical Information and Computer Sciences* 44, 2133–44.

Cao, X.-J., C.-R. Sun, and Y.-J. Pan. 2003. "The Complex of Flunixin and Meglumine." *Acta Crystallographica Section E: Structure Reports Online* 59, o1471. doi:10.1107/S1600536803019470.

Corradi, E., S. V. Meille, M. T. Messina, P. Metrangolo, and G. Resnati. 2000. "Halogen Bonding Versus Hydrogen Bonding in Driving Self-Assembly Processes." *Angewandte Chemie International Edition* 39: 1782–86.

Crystal Impact. 2022. Diamond. V. 4.6.8. Windows. Crystal Impact – Dr. H. Putz & Dr. K. Brandenburg.

Dassault Systèmes. 2021. *Materials Studio. V. 2021*. Windows. BIOVIA, San Diego, CA.

Di Fabio, R., G. Alvaro, B. Bertani, D. Donati, S. Giacobbe, C. Marchioro, C. Palma, and S. M. Lynn. 2002. "Novel Stereocontrolled Addition of Allylmetal Reagents to α-Imino Esters: Efficient Synthesis of Chiral Tetrahydroquinoline Derivatives." *Journal of Organic Chemistry* 67, 7319–28. doi:10.1021/jo020327d.

Dizendorf, E. V., V. Treyer, G. K. Von Schulthess, and T. F. Hany. 2002. "Application of Oral Contrast Media in Coregistered Positron Emission Tomography—CT." *American Journal of Roentgenology* 179, 477–81. doi:10.2214/ajr.179.2.1790477.

Donnay, J. D. H., and D. Harker. 1937. "A New Law of Crystal Morphology Extending the Law of Bravais." *American Mineralogist* 22, 446–47.

Dovesi, R., A. Erba, R. Orlando, C. M. Zicovich-Wilson, B. Civalleri, L. Maschio, M. Rérat, S. Casassa, J. Baima, S. Salustro, and B. Kirtman. 2018. "Quantum-Mechanical Condensed Matter Simulations with CRYSTAL." *Wiley Interdisciplinary Reviews: Computational Molecular Science* 8, e1360.

Favre-Nicolin, V., and R. Černý. 2002. "FOX, 'Free Objects for Crystallography: A Modular Approach to Ab Initio Structure Determination from Powder Diffraction'." *Journal of Applied Crystallography* 35, 734–43.

FDA.gov. 2017. 'MD-76®R', 1–20.

Friedel, G. 1907. "Etudes Sur La Loi De Bravais." *Bulletin de Minéralogie* 30, 326–455.

Fucke, K., J. A. K. Howard, and J. W. Steed. 2012. "Overcoming the Solvation Shell During the Crystallisation of Diatrizoic Acid from Dimethylsulfoxide." *Chemical Communications* 48, 12065–67. doi:10.1039/c2cc35995b.

Fucke, K., G. J. McIntyre, M.-H. Lemee-Cailleau, C. Wilkinson, A. J. Edwards, J. A. K. Howard, and J. W. Steed. 2015. "Insights into the Crystallisation Process from Anhydrous, Hydrated and Solvated Crystal Forms of Diatrizoic Acid." *Chemistry - A European Journal* 21, 1036–47. doi:10.1002/chem.201404693.

Gates-Rector, S., and T. N. Blanton. 2019. "The Powder Diffraction File: A Quality Materials Characterization Database." *Powder Diffraction* 39, 352–60.

Gatti, C., V. R. Saunders, and C. Roetti. 1994. "Crystal-Field Effects on the Topological Properties of the Electron-Density in Molecular Crystals – The Case of Urea." *Journal of Chemical Physics* 101, 10686–96.

Geng, L., R. Wu, H. Hu, Y. Zhao, L. Fan, Z. Zhao, D. Liao, M. Li, M. Xiang, Y. Ma, and X. Du. 2018. "Clinical Application of Oral Meglumine Diatrizoate Esophagogram in Screening Esophageal Fistula During Radiotherapy for Esophageal Cancer." *Medicine* 97, e0668. doi:10.1097/MD.0000000000010668.

Groom, C. R., I. J. Bruno, M. P. Lightfoot, and S. C. Ward. 2016. "The Cambridge Structural Database." *Acta Crystallographica Section B: Structural Science, Crystal Engineering and Materials* 72, 171–79.

Hirshfeld, F. L. 1977. "Bonded-Atom Fragments for Describing Molecular Charge Densities." *Theoretica Chemica Acta* 44, 129–38.

Kaduk, J. A., C. E. Crowder, K. Zhong, T. G. Fawcett, and M. R. Suchomel. 2014. "Crystal Structure of Atomoxetine Hydrochloride (Strattera), $C_{17}H_{22}NOCl$." *Powder Diffraction* 29, 269–73.

Kresse, G., and J. Furthmüller. 1996. "Efficiency of Ab-Initio Total Energy Calculations for Metals and Semiconductors Using a Plane-Wave Basis Set." *Computational Materials Science* 6, 15–50.

Laun, J., and T. Bredow. 2022. "BSSE-Corrected Consistent Gaussian Basis Sets of Triple-Zeta Valence with Polarization Quality of the Fifth Period for Solid-State Calculation." *Journal of Computational Chemistry* 43, 839–46. doi:10.1002/jcc.26839.

Lee, P. L., D. Shu, M. Ramanathan, C. Preissner, J. Wang, M. A. Beno, R. B. Von Dreele, L. Ribaud, C. Kurtz, S. M. Antao, X. Jiao, and B. H. Toby. 2008. "A Twelve-Analyzer Detector System for High-Resolution Powder Diffraction." *Journal of Synchrotron Radiation* 15, 427–32.

Macrae, C. F., I. Sovago, S. J. Cottrell, P. T. A. Galek, P. McCabe, E. Pidcock, M. Platings, G. P. Shields, J. S. Stevens, M. Towler, and P. A. Wood. 2020. "*Mercury 4.0*: From Visualization to Design and Prediction." *Journal of Applied Crystallography* 53, 226–35.

Materials Design. 2016. MedeA. V. 2.20.4. Windows.

Mayo Clinic, Mayo Foundation for Medical Education and Research 2022. "Diatrizoate (Intravenous Route) Side Effects." https://www.mayoclinic.org/drugs-supplements/diatrizoate-intravenous-route/side-effects/drg-20150982?p=1.

Najib, M. N. M., K. Back, and K. Edkins. 2017. "The Complex Solid-State Landscape of Sodium Diatrizoate Hydrates." *Chemistry - A European Journal* 23, 17339–47. doi:10.1002/chem.201703658.

O'Boyle, N. M., M. Banck, C. A. James, C. Morley, T. Vandermeersch, and G. R. Hutchison. 2011. "Open Babel: An Open Chemical Toolbox." *Journal of Chemical Informatics* 3, 33. doi:10.1186/1758-2946-3-33.

Raines, J. 2008. "Oral Contrast and Method of Producing the Oral Contrast." United State Patent 7,384,624 B2.

Rammohan, A., and J. A. Kaduk. 2018. "Crystal Structures of Alkali Metal (Group 1) Citrate Salts." *Acta Crystallographica Section B: Crystal Engineering and Materials* 74, 239–52. doi:10.1107/S2052520618002330.

Spackman, P. R., M. J. Turner, J. J. McKinnon, S. K. Wolff, D. J. Grimwood, D. Jayatilaka, and M. A. Spackman. 2021. "Crystalexplorer: A Program for Hirshfeld Surface Analysis, Visualization and Quantitative Analysis of Molecular Crystals." *Journal of Applied Crystallography* 54, 1006–11. doi:10.1107/S1600576721002910; https://crystalexplorer.scb.uwa.edu.au.

Stephens, P. W. 1999. "Phenomenological Model of Anisotropic Peak Broadening in Powder Diffraction." *Journal of Applied Crystallography* 32, 281–89.

Sykes, R. A., P. McCabe, F. H. Allen, G. M. Battle, I. J. Bruno, and P. A. Wood. 2011. "New Software for Statistical Analysis of Cambridge Structural Database Data." *Journal of Applied Crystallography* 44, 882–86.

Toby, B. H., and R. B. Von Dreele. 2013. "GSAS II: The Genesis of a Modern Open Source All Purpose Crystallography Software Package." *Journal of Applied Crystallography* 46, 544–49.

van de Streek, J., and M. A. Neumann. 2014. "Validation of Molecular Crystal Structures from Powder Diffraction Data with Dispersion-Corrected Density Functional Theory (DFT-D)." *Acta Crystallographica Section B: Structural Science, Crystal Engineering and Materials* 70, 1020–32.

Wang, J., B. H. Toby, P. L. Lee, L. Ribaud, S. M. Antao, C. Kurtz, M. Ramanathan, R. B. Von Dreele, and M. A. Beno. 2008. "A Dedicated Powder Diffraction Beamline at the Advanced Photon Source: commissioning and Early Operational Results." *Review of Scientific Instruments* 79, 085105.

Wavefunction, Inc. 2020. *Spartan '18. V. 1.4.5*. Wavefunction Inc., Irvine, CA.

Wavefunction, Inc. 2022. *Spartan '20. V. 1.1.4*. Wavefunction Inc., Irvine, CA.

Weil, M., and K. N. Morris 2004. "Pharmaceuticaly Enhanced Low-Energy Radiosurgery." United States Patent Application 2004/0006254 A1 92004).

Wheatley, A. M., and J. A. Kaduk. 2019. "Crystal Structures of Ammonium Citrates." *Powder Diffraction* 34, 35–43.

Wilcken, R., M. O. Zimmermann, A. Lange, A. C. Joerger, and F. M. Boeckler. 2013. "Principles and Applications of Halogen Bonding in Medicinal Chemistry and Chemical Biology." *Journal of Medicinal Chemistry* 56: 1363–88.